

Interaction of Human Mesenchymal Stem Cells with Soft Nanocomposite Hydrogels Based on Polyethylene Glycol and Dendritic Polyglycerol


Rotsiniaina Randriantsilefisoa,* Yong Hou, Yuanwei Pan, José Luis Cuellar Camacho, Michaël W. Kulka, Jianguang Zhang, and Rainer Haag*

Keeping the stemness of human mesenchymal stem cells (hMSCs) and their adipocyte differentiation potential is critical for clinical use. However, these features are lost on traditional substrates. hMSCs have often been studied on stiff materials whereas culturing hMSCs in their native niche increases their potential. Herein, a patterned hydrogel nanocomposite with the stiffness of liver tissues is obtained without any molding process. To investigate hMSCs' mechanoresponse to the material, the RGD spacing units and the stiffness of the hydrogels are dually tuned via the linker length. This work suggests that hMSCs' locomotion is influenced by the nature of the hydrogel layer (bulk or thin film). Contrary to on bulk surfaces, cell traction occurs during cell spreading on thin films. In addition, hMSCs' spreading behavior varies from shorter to longer linker-based hydrogels, where on both surfaces hMSCs maintains their stemness as well as their adipogenic differentiation potential with a higher number of adipocytes for nanocomposites with a longer polymer linker. Overall, this work addresses the need for a new alternative for hMSCs culture allowing the cells to differentiate exclusively into adipocytes. This material represents a cell-responsive platform with a tissue-mimicking architecture given by the mechanical and morphological properties of the hydrogel.

1. Introduction

Mesenchymal stem cells are multipotent cells with a high expansion ability and multilineage differentiation.^[1] In recent years, they are being used in a number of applications, i.e., cell-based therapy,^[2,3] tissue engineering,^[4–6] and regenerative medicine.^[7,8] Since the work of Fridenstein in 1976, stiff materials are used for stem cell culturing, typically tissue culture plates (TCPS) or glass substrates.^[9] However, it has been reported in the literature that

R. Randriantsilefisoa, Y. Hou, Y. Pan, Dr. J. L. C. Camacho, M. W. Kulka, Dr. J. Zhang, Prof. R. Haag
Institut für Chemie und Biochemie
Freie Universität Berlin
Takustr. 3, 14195 Berlin, Germany
E-mail: rani2f@zedat.fu-berlin.de, lycon624@live.fr;
haag@chemie.fu-berlin.de

 The ORCID identification number(s) for the author(s) of this article can be found under <https://doi.org/10.1002/adfm.201905200>.

© 2019 The Authors. Published by WILEY-VCH Verlag GmbH & Co. KGaA, Weinheim. This is an open access article under the terms of the Creative Commons Attribution License, which permits use, distribution and reproduction in any medium, provided the original work is properly cited.

DOI: 10.1002/adfm.201905200

stem cells have responded to their mechanical and biochemical environment.^[10–16] As an example, different stiffnesses can lead to different lineage specifications and cell morphologies; a stiff surface will more likely lead to osteoblasts while a softer surface will lead to adipocytes, neurons, or myoblasts.^[12] The cell morphology is also influenced by the microenvironment, where a flat or a patterned surface will give different cell phenotypes as well as different patterns, which lead to different cell shapes (elongated, round, star shaped, spheroids).^[17–19] In addition, the presence and distribution of cell promoters (proteins and peptides) such as RGD, fibronectin, and collagen on the surface will influence the cell fate and the interaction of the cell with the materials' surface through integrins for example.^[13]

Soft materials are sensitive and can undergo large deformation.^[20] As a result, mechanical instabilities of this type of materials exist and are numerous in nature.^[21] They are observable in the

brain, the skin, and in plants, to name a few examples.^[22] These instabilities result from environmental stimuli or constraints. For instance, instabilities of soft hydrogels anchored on a substrate are due to a high swelling constrained by the substrate.^[23–25] They are being more and more applied in diverse fields. For example, wrinkled hydrogels are used in adhesives,^[26] stretchable electronics,^[27] control of surface wettability,^[28] and moisture-responsive devices.^[29]

Furthermore, it has been suggested that soft substrates (≈ 1 – 10 kPa) could keep and/or recover the stemness of hMSCs after a limited amount of passages and postpone the senescence of the cells as opposed to a culture on TCPS (≈ 3 GPa). Typically, culturing methods of hMSCs are performed on TCPS, a hard type of surface, however, when cultured in vitro on such surface, the cells are likely to lose their proliferative and multilineage differentiation potential. Especially after several number of passages, usually after around the twelfth passage (P12) and multiple differentiation steps, they tend to go in a phase called “senescence” where the intrinsic function (stemness) of stem cells fades and cannot be recovered. This represents a major issue in tissue engineering where a culture system that maintains the stemness of the hMSCs is needed to efficiently expand them in vitro.^[30,31] The impact of

patterned surfaces on cellular behavior has also been investigated in recent years. Guvendiren and Burdick have reported the effect of lamellar or hexagonal wrinkled patterns on hMSC morphology and differentiation. They have suggested that, depending on the pattern and on where the cells are located on the pattern, hMSCs remain round or spread and are differentiated into osteogenic or adipogenic lineages.^[29] Furthermore, most organs and tissues are soft materials. Physicochemical properties as well as the appropriate mechanical properties are crucial for an optimal culture system for such cells.^[32] For these reasons, patterned soft surfaces could be an alternative structure for tissue engineering applications.

The use of antifouling surfaces such as polyethylene glycol hydrogels in tissue engineering have numerous advantages, i.e., the stiffness can be tuned with the PEG length. Furthermore, their antifouling property will prevent unspecific protein adsorption.^[33] Nevertheless, some publications reported the inability of cells to adhere on soft hydrophilic surfaces even in the presence of RGD. First, the high hydrophilicity of some bare surfaces can prevent cell adhesion. Another reason is the lack of exposure of the peptides to the cells.^[34] Ding et al. have shown that culturing cells on such antifouling surface was possible only by having the optimal spacing of functional proteins or peptides. They found that a critical local inter-ligand spacing of RGD of ≈ 70 nm is necessary for cell attachment. Their work consisted, inter alia, in nanopatterning a hydrogel surface with RGD bearing AuNP where cell attachment could be observed.^[35–37] AuNPs are now a standard feature of particle because of their stability, their easy synthesis, and their high loading density of functionalities.^[38,39] They can then represent multiple anchoring points to proteins, peptides, and other biomolecules, which are useful for cell adhesion, proliferation, and differentiation.^[40] The size of AuNPs is tunable as well as

their density within the material. They are biocompatible in a reasonable concentration and well suitable for cell culture. The ultimate advantage of having nanocomposites is that the nanoparticles can be attached through Au–S chemistry, they are efficient and stable and do not allow any leaching of the particles out of a hydrogel structure. These nanocomposites therefore prevent the biomolecules from escaping the network and consequently avoid a loss of function or instability of the matrix.^[41]

Soft tissue replacement is necessary in case of soft tissue pathologies, injuries, trauma, or defects. For example, adipose tissue defects and pathologies represent a challenge in reconstructive medicine. This issue has led to the emerging field of soft tissue engineering, which aims to provide a biologic substitute that promotes soft tissue growth and regeneration.^[42–45]

In this study, the interaction of hMSCs culture with the surface of a soft hydrogel nanocomposite ($G' < 2$ kPa) was investigated. To achieve this aim, a hydrogel nanocomposite with a highly porous and interconnected structure, in principle adequate for cell adherence and culture was produced. This material is inert to biochemical change, nontoxic, and transparent. The differentiation potential of hMSCs along with the spreading, immunophenotyping, and mechanosensibility on two differently RGD-spaced hydrogels was investigated (Figure 1).

2. Results and Discussion

2.1. Synthesis and Fabrication of Hydrogel Nanocomposites with Different Types of Surface Patterns

Surface topography is crucial for stem cell proliferation and fate. Surface morphology associated with cell adhesive ligands is beneficial for stem cells spreading. Especially, topography

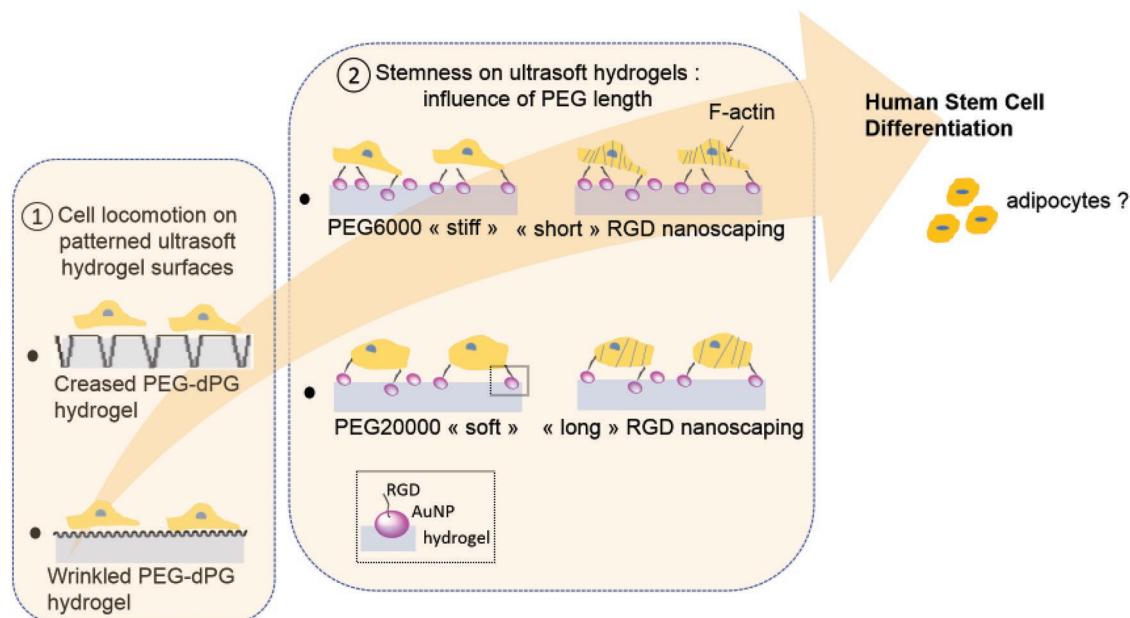


Figure 1. Schematic representation of the following study aiming: first to investigate the effect of patterns (wrinkles or creases) on cell locomotion and second the effect of the stiffness (keeping it in the soft region) and spatial organization of cell-adhesive peptides on adhesion, cell morphology, and conservation of intrinsic functions of hMSCs (mechanosensing ability, immunophenotyping, and differentiation capability).

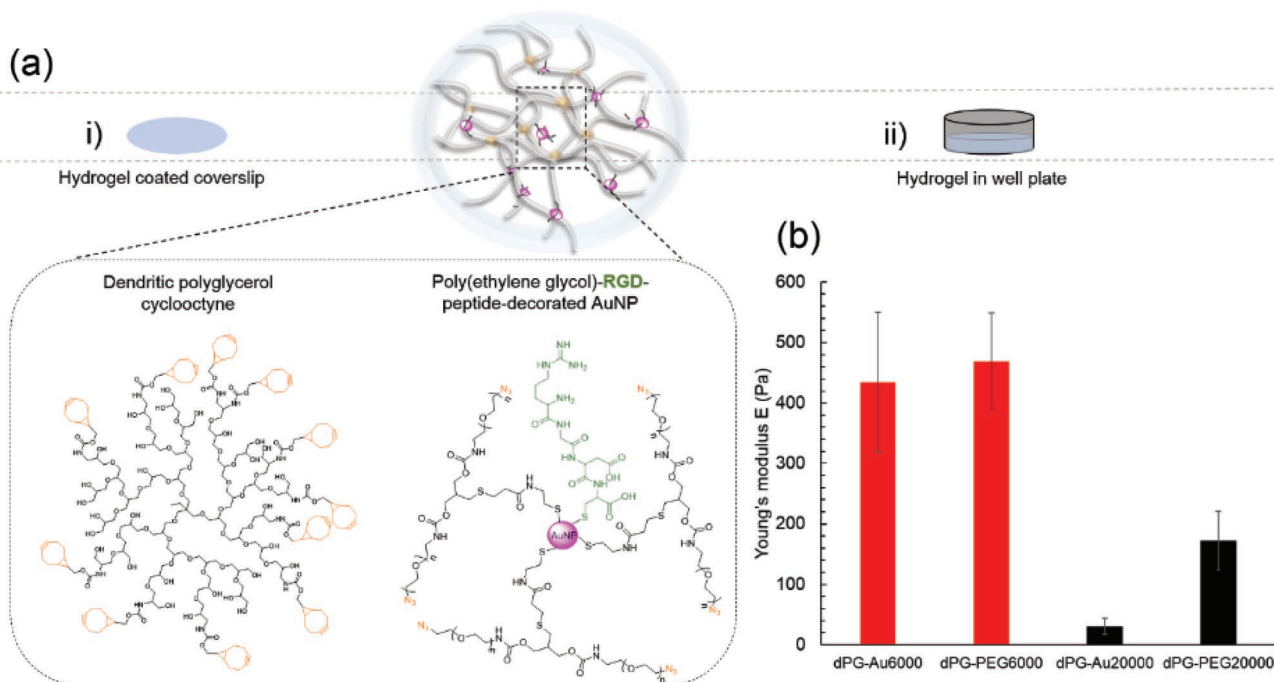


Figure 2. Synthesis and rheological characterization of hydrogels. a) Representation of the hydrogel network composed of clicked functional PEG, RGD–AuNP, and dPG-based nanocomposite hydrogel. Functionalized macromolecular precursors: dendritic polyglycerol cyclooctyne (dPG MW 10 kDa, 10% cyclooctyne functionality), diazide-functionalized PEG linker with different molecular weights (6000 Da and 20 000 Da) form 3D hydrogel structures via the SPAAC reaction. Thiol-containing PEG linker and RGD peptides are conjugated to the gold nanoparticles by means of thiol–Au reaction. This forms in the end a nanocomposite hydrogel network with immobilized RGD peptides and PEG linkers as well as AuNP in the network. Hydrogels are either (i) covalently attached on glass coverslips via silane moieties on glass surfaces or (ii) directly deposited in a well plate. b) Shear elastic modulus of hydrogels made-up of dPG, and PEG of a molecular weight 6000 or 20000 with RGD-bearing AuNP, called “dPG-Au-6000,” “dPG-Au-20000,” or without RGD-bearing AuNP, called “dPG-PEG-6000,” “dPG-PEG-20000.”

of the surface enhances the differentiation of hMSCs toward osteogenic and adipogenic lineage.^[29,30] Previous studies have suggested that the combined micro- and nanoscale topography is favoring hMSCs proliferation and differentiation.^[46,47] To form patterned hydrogel nanocomposites (Figure 2), we used our previously reported hydrogel fabrication approach, with some modifications.^[48] In these systems, copper-free, strain-promoted alkyne–azide click reaction (SPAAC) and Au–S chemistry are used. This bioorthogonal gel formation strategy is a spontaneous and efficient way that occurs in mild conditions. PEG is the linker, crosslinked with dendritic polyglycerol (dPG) and AuNP. This forms a nanocomposite hydrogel with RGD-bearing AuNP, and dPG connected through flexible PEG chains. RGDs possess a supplementary cysteine group and a supplementary thiol group was also inserted in the middle part of the PEG chain via EDC/NHS coupling (detailed synthesis is presented in the Supporting Information). PEG and RGD are anchored on the AuNP via the binding of their thiol functional groups to the AuNP. PEG and dPG are used for their nonfouling properties to avoid unspecific protein adsorption. Characterization of the composition in AuNPs and their spatial organization are presented in SI (Figures S6, S7, and S11, Supporting Information).

The stiffness of the hydrogel as well as the RGD spacing units will be tuned by the PEG length. The stiffness might also be influenced by the molecular weight of dPG (crosslinker), which was kept constant at 10 kDa in this study. Since the RGD

peptides are anchored on the AuNP and AuNPs are bound to the PEG linkers, the RGD spacing unit will also be therefore influenced by the PEG length (Figure S14D, Supporting Information).

To get two types of instabilities on the surface of the hydrogels, two methods have been used, either spin coating the hydrogel solution on a silanized glass coverslip to covalently anchor a thin hydrogel film onto a glass substrate or a simple deposition of the hydrogel solution in a tissue culture plate to get a thick hydrogel layer in a well. The anchoring step is crucial as well as the presence of an aqueous environment to obtain the patterns. By depositing hydrogel solutions on two types of substrates to form a hydrogel layer, and then immersing the material in aqueous medium, we expect to naturally produce hydrogel surfaces with two different topographies. Furthermore, these hydrogels, as soft materials with high swelling capacities^[48] (Figure S8, Supporting Information), expand tremendously in the presence of medium because of the difference in osmotic pressure in the hydrogel and in the aqueous environment. The more swollen the hydrogels are, the higher stress response they give resulting from the constraint applied by the substrate.^[23,49] We chose to observe the wrinkled surface morphology by atomic force microscopy and the creased surface by phase contrast optical microscopy. We adapted the imaging technique to the size of the patterns and to the feasibility of the method (due to substrate restrictions, AFM images of the creased surface could not be obtained).

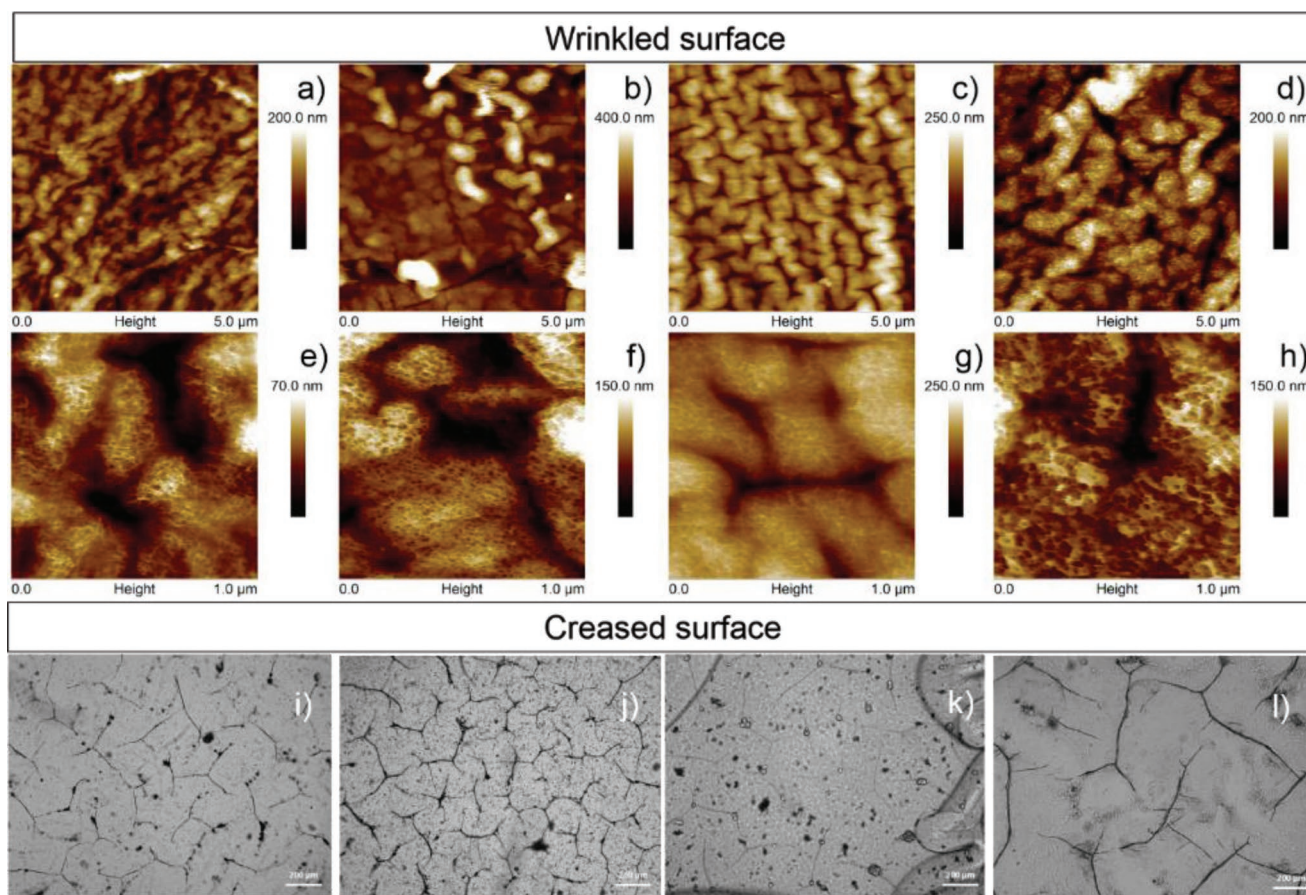


Figure 3. Surface characterization showing the hydrogel patterns on both a–h) coverslip and i–l) well plate. Characterization of coverslips coated with a thin hydrogel layer was done by AFM with a) dPG–Au6000, b) dPG–Au20000, c) dPG–PEG-6000, d) dPG–PEG20000, with the respective zoom in (e–h). All surfaces present micro- and nanoroughness. Hydrogels deposited on well plates were characterized by i–l) phase contrast optical imaging, with i) dPG–Au6000, j) dPG–Au20000, k) dPG–PEG-6000, l) dPG–PEG20000. Wrinkles appear on (a–h) due to a constraint swelling in one direction and creases on (i–l) due to constrained swelling in two directions. Scale: (i–l): 200 μm .

In **Figure 3** and **Figure S3** (Supporting Information), optical micrographs of the thin hydrogel film after immersion in aqueous medium are shown. These representations of the surfaces of the thin hydrogel films (2D and 3D views, respectively) show a homogeneously wrinkled morphology with micro- and nanoroughness of around between 27 to 310 nm (micro-) and 4 to 57 nm (nano-) (**Table 1** and **Figure 4**). AFM images $1\ \mu\text{m} \times 1\ \mu\text{m}$ also testify the presence of interconnected pores at the nanoscale and a mesh size of around 14 to 20 nm for dPG–Au6000 and a larger mesh for dPG–Au20000 of around 30 nm.

Appealingly, the visible patterns obtained resemble quite closely to the ones of the brain. Brain patterns have been explained by the soft nature of the organ that is constrained by a hard “substrate” that is the surrounding (the skull). During the development of the brain, the cerebral cortex displays a high expansion and the constraint of the stiff environment leads to folding and consequently gives wrinkled patterns.^[2,50] The same phenomenon explains the wrinkles obtained for these hydrogels.

In contrast, the optical microscope images (**Figure 3i,j**) obtained in the case of a hydrogel deposited in a well plate and

Table 1. Surface characterization of the hydrogels in terms of roughness and PEG chain size in the hydrogel matrix described by the pore and mesh sizes by AFM and rheological measurements.

Hydrogels	Micro- R_q [nm] ^{a)}	Micro- R_{qmax} [nm] ^{a)}	Nano- R_q [nm] ^{a)}	Nano- R_{qmax} [nm] ^{a)}	Pore diameter [nm] ^{a)}	Mesh size [nm] ^{b)}
dPG–Au6000	27.5 ± 6.7	126.3 ± 32.6	4.5 ± 0.3	19.2 ± 3.2	15.6 ± 3.1	13 ± 1
dPG–Au20000	71.1 ± 30.7	309.4 ± 100.1	8.6 ± 3.4	33.9 ± 10.3	19.1 ± 5.4	14 ± 0.5
dPG–PEG6000	36.4 ± 7.6	167.6 ± 26.1	6.6 ± 1.4	30.9 ± 5.8	16.9 ± 4.4	31 ± 8
dPG–PEG20000	44.2 ± 8.6	207 ± 28	14.1 ± 1.6	56.5 ± 10.1	26.7 ± 3.9	18 ± 2

^{a)}By atomic force microscopy; ^{b)}By rheological measurements.

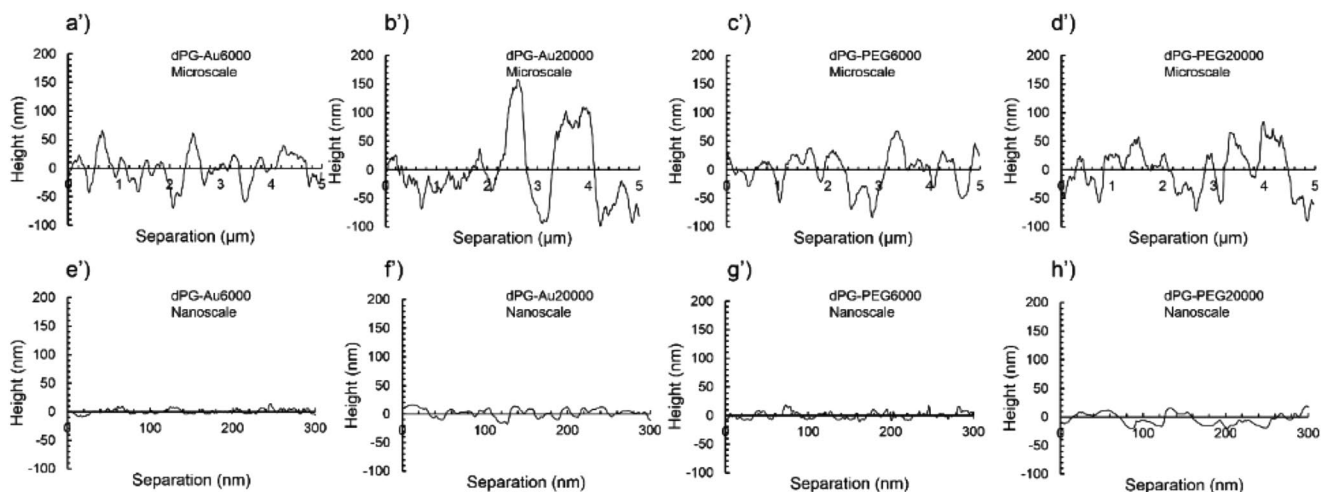


Figure 4. Cross section profiles of the hydrogels surface where two different roughness are visible. a') dPG-Au6000, b') dPG-Au20000, c') dPG-PEG6000, and d') dPG-PEG20000 show microroughness, while e'–h') are the corresponding profiles where nanoroughness is visible when imaging is at higher magnification.

observed after hydration, show creased surfaces, very similar to the patterns obtained by Trujillo et al.^[51] The patterned morphologies were evaluated after swelling the films or thick layers in medium. It is notable that in dry state, no patterns are seen, which shows that the wrinkles or creases only appear by hydration. Prior to immersion in a solvent, the material is stress free. After immersion, the hydrogels undergo an osmotic stress due to the solvent with polymer chains and counter ions imbalance. But this bounces back by an elastic stress while the polymer chains are stretching. Moreover, when a mechanical limitation is applied such as an anchoring on a hard substrate, the hydrogels can only expand on a specific direction. As they are constrained by two directions by the walls of the well and the bottom of the well, only the normal direction to the bottom of the substrate will be available for the hydrogel to expand in the presence of the medium. The response to this stress will be, when the stress reaches a critical point, a relaxation, after which the visible osmotically driven patterns appear (schematically explained in Figure S4b, Supporting Information). The characteristic spacing between folds is proportional to the thickness of the gel.^[51] When the hydrogel is constrained by only one direction by the substrate, the swelling in principle anisotropic will only be possible in the two other directions instead of the usual three in the absence of the substrate, which results in an equibiaxial compressive stress (schematically explained in Figure S4a, Supporting Information). This is also in accordance with other previously reported literature of soft hydrogels displaying surface instabilities.^[22,52–53]

The material properties of hydrogels were obtained by AFM through externally applied deformations with two differently shaped probes and their respective contact models. To test micro-mechanical properties, colloidal force spectroscopy (CFS) was used, while a bare sharp AFM tip was used to investigate the hydrogel mechanical behavior at the nanoscale. To obtain information of the material properties of swollen hydrogels, two main approaches were followed. Their mechanical response to external applied forces was tested by means of micro and nanoindentations using a colloidal probe and a bare sharp AFM tip.

2.2. hMSCs' Locomotion on the Wrinkled or Creased Hydrogel Nanocomposites

Cells can sense the mechanical properties of their surroundings because of several cellular events.^[56] The adhesion of a cell involves physical and chemical messengers, binding receptors, as well as the cytoskeleton. For example, in the cytoskeleton, the F-actins need to be polymerized by α -actinins to form a solid cell structure.^[57,58] Cell locomotion and focal adhesions are regulated by substrate flexibility. Rates of cell motility and lamellipodial activity increase on softer substrates more than stiffer ones.^[59] This is due to a reduced amount of phosphotyrosine at their adhesion sites when cultured on soft substrates.^[58] In this part, we intend to study the interaction of hMSCs with the hydrogel nanocomposite toward two different types of instabilities and to investigate the effects of the patterns on stem cells locomotion. hMSCs were cultured on two types of substrates: glass coverslips coated with thin hydrogel films ($\approx 0.1 \mu\text{m}$, swollen) and tissue culture plates coated with a thick hydrogel layer ($\approx 2 \text{mm}$, swollen). The thin layer of wrinkled hydrogel composite was attached to a glass coverslip and deposited in a 24-well plate to facilitate handling. In both substrates were cultured hMSCs for 72 h in DMEM with 10% FBS and 1% PS.

Figure 6 shows phase contrast optical images of the hydrogels surfaces with seeded hMSCs: a) the wrinkled thin hydrogel film with RGD–AuNP in the matrix, b) the corresponding creased hydrogel at a same magnification, and c) a control hydrogel without RGD–AuNP. These images show that in both cases with RGD–AuNP the cells adhered to the hydrogels. More interestingly, the cells were adhering where the wrinkles or creases were present. Additionally, these images testify of the strong cell attachment to the hydrogel films in the presence of RGD and where additional wrinkles appear as a consequence of the cellular contractile forces on the thin hydrogel sheets of crosslinked polymers after the cells have spread and crawled on the surface. As seen on Figure 6d, the cells, by spreading out on such a thin film, exerted a traction force that resulted in a compression of the material by the cells and stretched into radial wrinkles surrounding the cells.

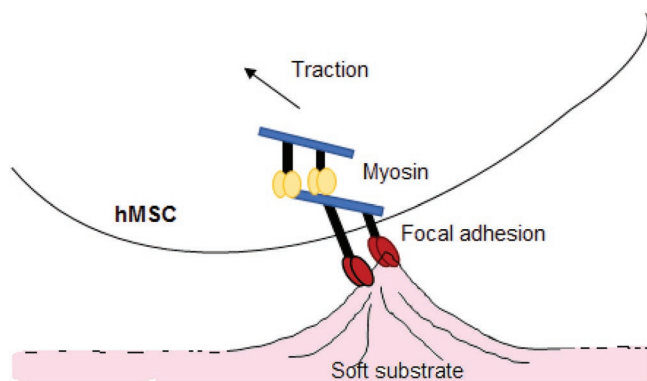


Figure 5. Schematic representation of traction force applied by cell locomotion on soft substrates. Cells pull against the substrate and significantly deform it by myosin contraction.

The surrounding of the cells is compressed by pulling out of the substrate toward them, radiating several wrinkles oriented along the axis of the tension and in this way, also linking the cell to the neighboring ones displaying the same phenomenon around them, creating a web like structure where many cells are interconnected. This wrinkling effect formed as a result of cell traction exerted beneath the cells as opposed to along the edges of the cells. Cells pull substrates through myosin contractions at 20 to 120 nm s⁻¹, resulting in deformations inversely proportional with stiffness (Figure 5). This phenomenon has been previously reported on other types of thin polymeric sheets and has been applied for example in cellular force microscopy.^[60–62]

In the case of the hydrogels deposited in a well plate displaying creases on the surface, the cells are preferentially oriented toward the creases. We hypothesized that they fell preferentially along the creases due to a higher surface area allowing a larger adhesion site resulting in higher focal adhesion expression. This cell behavior is supported by previous studies of creased surfaces for cell culture substrates showing cells migrating to the creases during cell culture.^[49] Fortunately, the cells mainly spread along each crease and displayed another type of cell spatial arrangement compared to the ones previously observed on the wrinkled patterns (Figure 6e). The cells gathered along a crease and promoted a tissue-like formation by being close to one another.

On the contrary, when hMSCs are cultured on a surface in absence of RGD (Figure 6f), they form spheroids, which indicates that hMSCs' adhesion was specifically mediated by interactions with RGD peptides that are present on the nanoparticles. These observations prove that the patterns on the surface of the same nanocomposite influence the cells locomotion and interaction with the substrate and the presence of RGD is crucial for cell adhesion thus spreading. It is important to point out that these surfaces are reusable. After trypsinization, and washing, the surface can host new cells again.

2.3. hMSCs' Spreading Is Influenced by the Substrate's Mechanical Properties

After showing that hMSCs strongly adhere to the hydrogels, next we focus on the influence of a variation of the PEG length,

thus a change in stiffness and RGD spacing units, keeping the type of substrate constant (thin hydrogel film). We compared the spreading behavior of the cells on the nanocomposites surface to standard methods of culturing hMSC on hard surfaces, and on soft polyacrylamide hydrogels, here called "PAAm₆₀₀₀" and "PAAm₂₀₀₀₀" (with G' (PAAm₆₀₀₀) ≈ 1400 Pa and G' (PAAm₂₀₀₀₀) ≈ 600 Pa). On tissue culture plate polystyrene (TCPS), hMSCs are known to lose their spindle morphology, and display a large spreading area with irregular shapes after a few passages and multiple differentiation steps.^[63] And yet, an enhanced spreading area is characteristic of a senescence state, in other words, an irreversible cell division arrest which makes the cells unsuitable for clinical use. This issue has been addressed and is still looking for a solution.^[30] In this part, we study two hydrogels: a system with PEG20000 having an average shear elastic modulus of around 600 Pa and a matrix with PEG6000 around twice as stiff, having an average shear elastic modulus of around 1400 Pa (Figure 2). These moduli are chosen to be in the range of organ tissues such as liver or kidney.^[32] Studying hMSCs in their native niche increases their potential for use in implants or substrates for tissue engineering.^[32] Interestingly, the RGD spacing distance and the stiffness of the matrix are related to the PEG length. In this matrix, several RGD peptides are bound to AuNP via Au–S bonds and AuNP are bound to the polymers via Au–S bonds with a thiol group present in the middle of the PEG linkers. This indicates that the interligand spacing is given by the length of the PEG linkers considering that each AuNP bears at least one RGD peptide. As a result, both parameters should be simultaneously considered. We hypothesized that since the RGD spacing has an influence on the cell spreading, as well as the stiffness, both are expected to influence the spreading altogether. Measurements of the hMSCs spreading areas (Figure 7) showed that hMSCs on a hydrogel with PEG20000 and with PEG6000 have a significant difference in spreading areas with a nanocomposite with PEG20000 (≈1500 μm²) smaller than the one with PEG6000 (≈2000 μm², with *p* < 0.001), but with similar cell morphologies being quite diverse, elongated, triarmed, and round. On the contrary, hMSCs on TCPS had a larger distribution of spreading areas with an average of ≈3000 μm² and the cells had flat and large shapes. The cells on PAAms have a limited spreading area of ≈250 μm², which is a proof of the effect of the mechanical properties of the surface and the RGD nanospacing regulating the cell behavior on the dPG–Au-based hydrogels. The hMSCs cytoskeletons on hydrogels differ from the ones seen on typical TCPS, thick elongated fibers without any actin dots are visible on the hard substrate whereas, on the dPG–Au-based hydrogels, the fibers are thinner, organized, and with a few actin dots, and on PAAm hydrogels, actin dots with only a few fibers are predominantly visible, as seen on Figure 7, Figure S14A,B (Supporting Information). Points of high fluorescence intensity are observed on the edge and a few on the hMSCs spread on dPG–Au-based hydrogels suggesting that focal adhesions points are around the cell and a few on the cells, certainly influenced by the RGD spatial organization. This structure was not observed for hMSCs on TCPS nor PAAm hydrogels. The differences in the shape of hMSCs' spreading on hydrogels are then due to the rearrangement of the actin filaments with a few dot shapes.

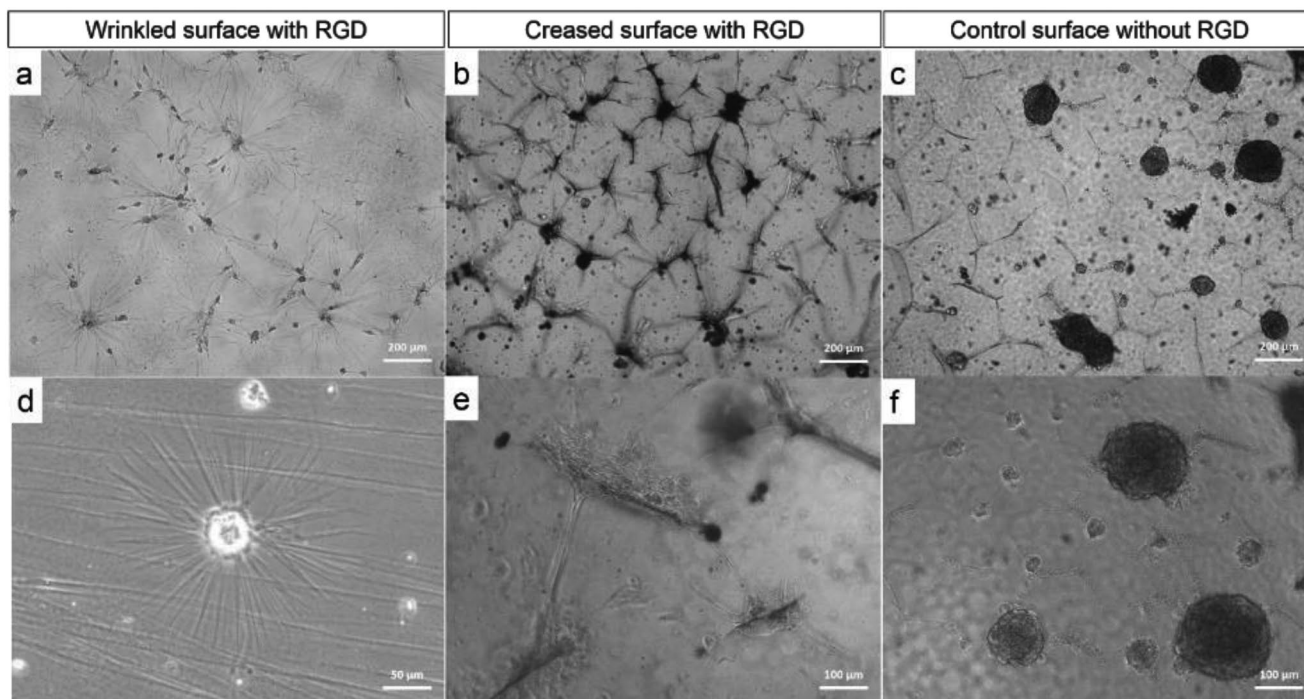


Figure 6. Phase contrast optical images of hMSCs cultured after 72 h with nanocomposite surfaces with or without RGD peptides. Representative low-resolution images of a) hydrogel with RGD peptide and AuNP, thin hydrogel film, b) hydrogel with RGD peptide and AuNP, bulk hydrogel, c) hydrogel without RGD nor AuNP. Representative high-resolution images of d) hydrogel with RGD peptide and AuNP, thin hydrogel film, e) hydrogel with RGD peptide and AuNP, bulk hydrogel, f) hydrogel without RGD nor AuNP. The low- and high-resolution images are taken on different areas of the same substrates. Observable additional wrinkling patterns produced by cellular traction forces on thin sheets of hydrogels cultured with hMSCs are on (d). The lines seen on the optical images (a) and (d) are stress wrinkles.

Since the staining assay only shows cell morphologies, in order to visualize the interaction of hMSCs at the interface of the dPG–Au-based hydrogels, we used SEM to image the cells (Figure 7a–h). We observed a strong attachment of the hMSCs on the surface with visible filopodia protrusions along the cells grabbing the surface since filopodia are the actin-rich part of cell useful for them to sense their environment to form adhesion sites to the material. This suggests that the cells are actively probing the surface to find adhesion points.

We intend to establish the link between what is observed from the cells on the different conditions to what is known in the literature to be able to speculate on the RGD spacing units of our system. It is reported in the literature that a small RGD spacing promotes the formation of an organized actin structure. The structured organization of the F-actin on both substrates implies that the RGD spacing is small enough, less than 70 nm, to form regularly crosslinked actin bundles.^[38,64] A critical number of integrins of five or six is necessary to cluster before getting a conformational change in the cytoplasm in the tail of the integrin, which builds up focal adhesion, talin, vinculin, and α -actinins. Frith et al. have established that above 44 nm RGD spacing, the cells start to develop filopodia to sense the RGDs on the surface.^[65,66] Therefore, we know from these observations that the RGD spacing units in our systems are between 44 and 70 nm. The difference in the RGD spacing between the two hydrogels is given by the PEG length and so, for PEG20000, the RGD

spacing is larger than the ones of a hydrogel with PEG6000, which is also confirmed by the mechanical characterization detailed in the previous sections that displayed a mesh size around twice as large for dPG–Au20000 compared to dPG–Au6000.

2.4. Stemness Remains on the Soft Hydrogel Nanocomposite: Hydrogels Keep the Mechanosensing Ability and Immunophenotypes of the hMSCs

According to the International Society for Cellular Therapy's standard criteria, in cell-based therapy, only CD73, CD90, and CD105-positive hMSCs are administered to patients in clinics.^[67,68] Culturing hMSCs on soft substrates (typically, $E \approx 10$ to 1 kPa) has been reported to be a better alternative to TCPS, keeping hMSCs' immunophenotyping intact.^[30,31] We intend to study these functions on soft substrates with topography. Stemness is characterized by the expression of these cell surface markers (CD73, CD90, CD105), meaning that the cell markers determine if there is a loss of differentiation potential.^[67,69] Expression of these markers on hMSCs cultured on the different surfaces has been assessed by confocal microscopy. In **Figure 8**, Figures S16 and S17 (Supporting Information), micrographs of the hMSCs on the different substrates and the corresponding FACS quantification are reported. The graphs obtained by FACS analysis, depicts the percentage of cell surface marker for the stemness CD73,

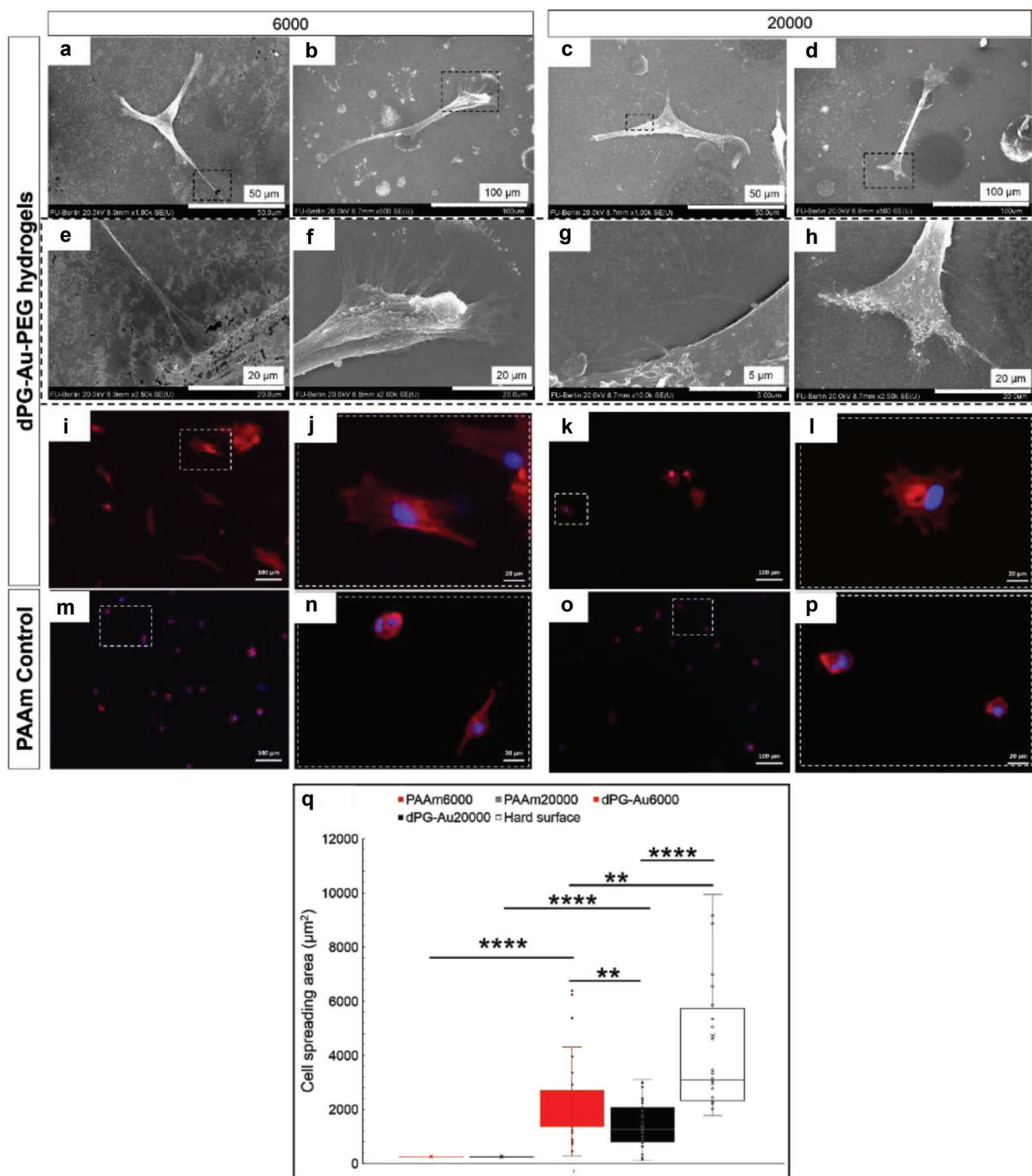


Figure 7. SEM images of hMSCs' strong interactions with a,b,e,f) dPG-Au-6000, c,d,g,h) dPG-Au-20000 hydrogels surface probing the environment by using filopodia. i,j) are the fluorescence images of hMSCs on dPG-Au-6000 and k,l) on dPG-Au-20000. m,n) are the fluorescence images of hMSCs on control soft PAAm hydrogel with a stiffness similar to dPG-Au-6000, o,p) are the fluorescence images of hMSCs on control soft PAAm hydrogel with a stiffness similar to dPG-Au-20000 q) is the quantification of the spreading area of the cells adhering to dPG-Au-6000 and dPG-Au-20000 hydrogels surface compared with a hard surface (TCPS). * $p < 0.05$, ** $p < 0.01$, *** $p < 0.001$, **** $p < 0.0001$; n.s., nonsignificant.

CD90, and CD105. For CD73, an increase of 37% is seen for cells seeded on the hydrogels compared to cells cultured on

TCPS. For CD90, an increase of 43% and for CD105, 79%. These results observed after 5 d of culture testify the strong

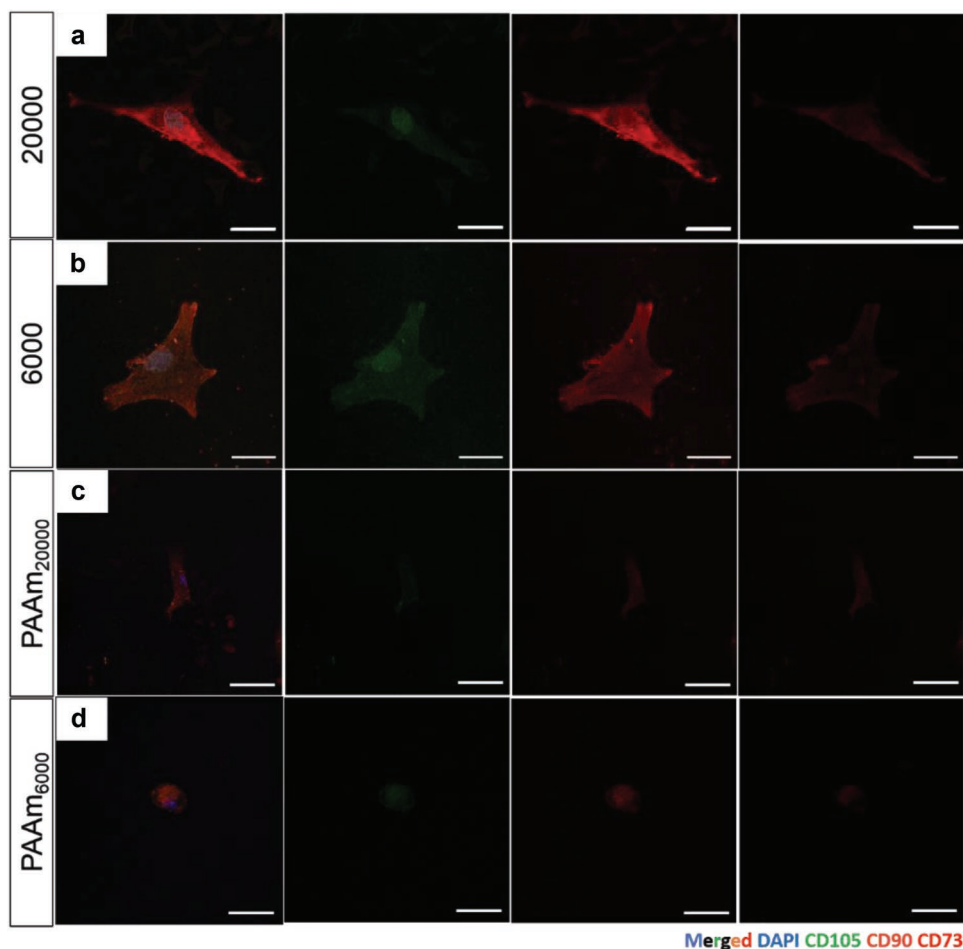


Figure 8. Immunophenotypic markers of hMSCs are kept with expansion on soft hydrogels. a,b) Immunofluorescence images of hMSCs on dPG–Au based hydrogels showing expression of CD105, CD73, CD90. c,d) are the respective PAAm hydrogel controls with PAAm₆₀₀₀ and PAAm₂₀₀₀₀ exhibiting the same stiffness as respectively dPG–Au6000 and dPG–Au20000. Immunofluorescence images of hMSCs on dPG–Au-based hydrogels showing strong expression of CD105, CD73, CD90 in dPG–Au-6000 and dPG–Au20000.

expression of the hMSCs on the soft hydrogels, where we observed a strong fluorescence in the cells for all the markers and on all the cells as opposed to on TCPS having only a slight fluorescence. The literature reports the percent of triple CD73, CD90, CD105 cells to be only 56% on TCPS.^[31] hMSCs are now being investigated in many applications in regenerative medicine, tissue engineering, and cell-based therapy. It is important to keep the stemness of the cells since a lower expression of the markers would decrease the efficiency of therapies.^[70–73] In line with immunophenotyping, mechanosensing ability is also a valued quality.^[74]

Yes-associated protein (YAP) is a transcription coactivator that serves as a sensor of the stiffness of the environment.^[75] YAP translocates to the nucleus when cells are cultured on stiff substrates and only on the cytoskeleton when on soft substrates.^[76] This way, by calculating the ratio between the YAP intensity between the nucleus and cytoplasm, we can estimate the degree of cell tension induced by the mechanical properties of microenvironment. After imaging and analysis of the YAP intensity on each cell (**Figure 9**), we observed that hMSCs cultured on TCPS exhibited a high YAP nuclear localization with a

Nuc/Cyt ratio of around 4 against only around 1 in the case of hMSCs on the soft hydrogels, also for the control PAAm hydrogels proving that the cells sense the soft property of the nanocomposite. The hydrogels had a positive impact on the transcriptional factor activity by favoring the retention of the mechanosensing ability of the hMSCs compared to on TCPS where they were unable to be sensitive to the microenvironment anymore after a few days. As the YAP influences the differentiation of the cells, based on these analyses, we investigated the differentiation potential of hMSCs on all the substrates in the next section.

Overall, TCPS appears to be a non-natural environment for hMSCs, especially when they keep their intrinsic functions such as immunophenotype and sensitivity to the mechanical properties of their microenvironment on softer substrates. This can be explained by the fact that a soft surface with tissue mimicking patterns displayed by the stress wrinkles mimics the natural cell environment, which then allowed them to restore their native functions. These native functions are crucial for the efficacy of therapies when administered in vivo.

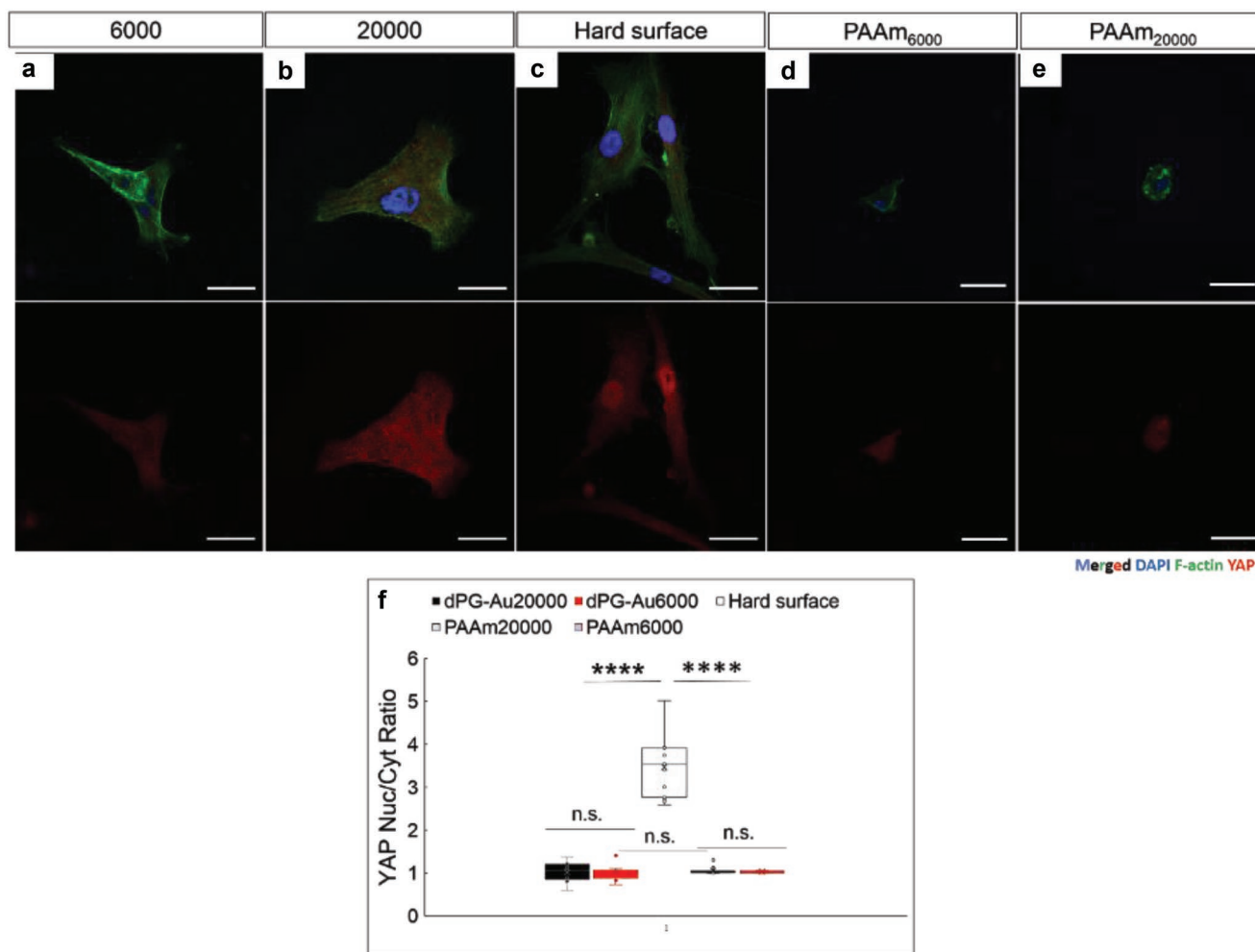


Figure 9. hMSCs mechanosensing ability on soft hydrogels as opposed to hard surfaces. a,b) Representative fluorescence images of hMSCs on dPG–Au nanocomposite hydrogels and c) Control hard substrate. d,e) Control PAAm hydrogels, with PAAm6000 and PAAm20000 exhibiting the same stiffness as respectively dPG–Au6000 and dPG–Au20000. f) Box plot reporting the YAP nuclear to cytoplasmic ratios of hMSCs cultured on dPG–Au hydrogels and control substrates. (* $p < 0.05$, ** $p < 0.01$, *** $p < 0.001$, **** $p < 0.0001$; n.s., nonsignificant).

2.5. hMSCs Can Differentiate Exclusively in Adipocytes on Tissue Mimicking Soft Hydrogels

hMSCs are involved in numerous treatments in various diseases due notably to their differentiation potential.^[77] We focus especially here on the adipogenesis potential for reconstructive medicine to cite only one example. Differentiating hMSCs specifically to one lineage specification represents a challenge.^[78] It is known that stiff substrates favor osteogenic differentiation with a less considerable adipogenic differentiation potential.^[26] Cells favor adipogenic differentiation on soft substrates with a round morphology.^[30,79] Normally, the hard surfaces would then be expected to produce osteoblasts and the adipogenic differentiation potential would vanish. In this section, we intend to compare the hMSCs differentiation behavior on the soft hydrogels with different nanospacing and hard substrates. To achieve this, the cells were seeded on the hydrogels and on TCPS in adipogenesis differentiation medium. Figure 9 is obtained after culture of hMSCs in adipogenesis medium after 17 d and staining each substrate with APL and Oil O

Red. We observed in the micrographs (Figure 10) that a hard substrate (typically TCPS) limited the adipose differentiation potential with only around 20% positive cells to adipogenesis in contrast to almost 80% of osteoblasts (in red for adipocytes and purple for osteoblasts), whereas, on the soft hydrogels, the adipose differentiation potential remains intact. We observed a higher number of adipose cells on a matrix with a longer PEG length (PEG 20000) with 85% cells differentiated compared to a hydrogel with PEG6000, with 60% positive cells. This can be explained by the conclusion of Wang et al. stating that differentiation was promoted by a larger nanospacing of RGD unit.^[35,80] As a hydrogel with a PEG20000 was supposed to have a larger nanospacing unit of RGD peptide, it might explain the difference in differentiation extent. We know that stem cell differentiation is influenced by both the RGD spacing units on the surface and stiffness of the substrates with a higher influence of RGD spacing. But in this case, both spacing and stiffness are expected then to lead simultaneously to an adipogenicity differentiation pathway since the matrix with PEG20000 is softer and with a larger RGD spacing. It is notable that only adipocytes

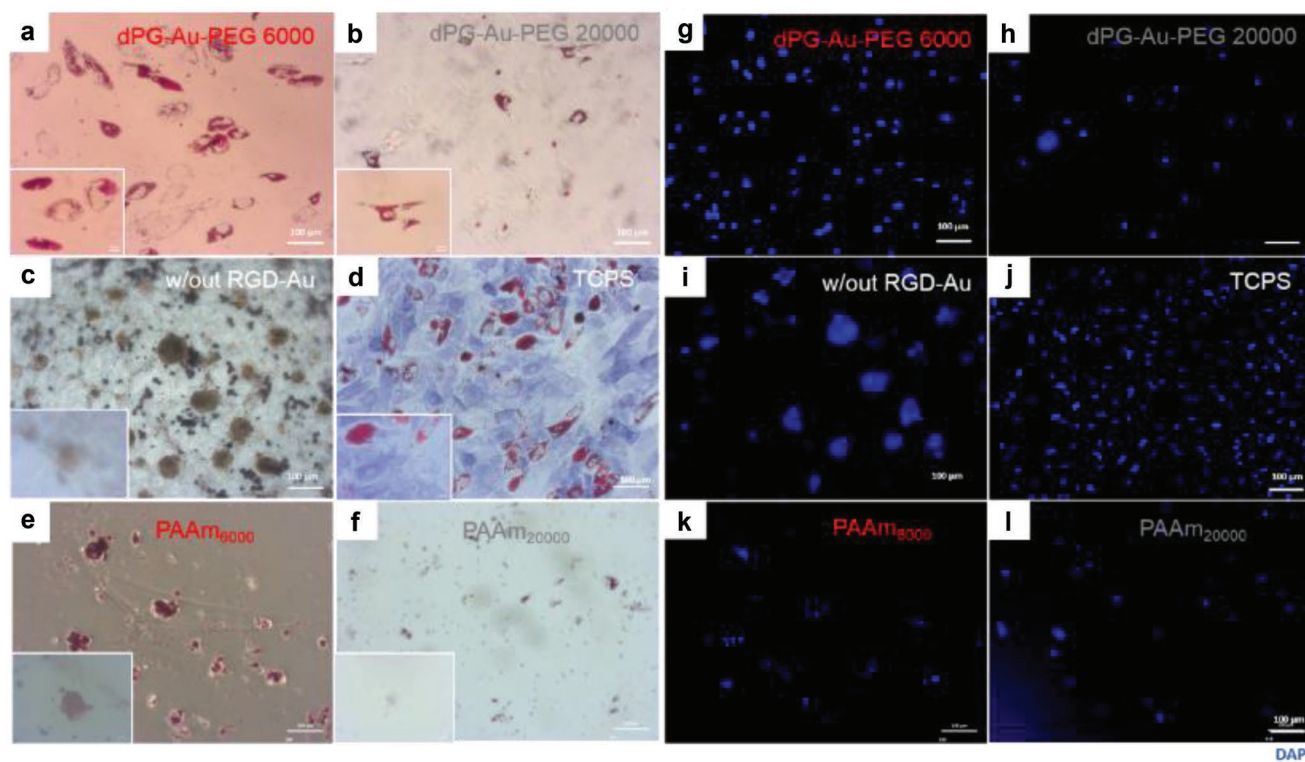


Figure 10. Adipogenic differentiation of cells adhering to hydrogels a) dPG–Au–PEG6000, b) dPG–Au–PEG20000, c) dPG–PEG, d) TCPS, e) PAAm₆₀₀₀, f) PAAm₂₀₀₀₀, with PAAm₆₀₀₀ and PAAm₂₀₀₀₀ exhibiting the same stiffness as respectively dPG–Au6000 and dPG–Au20000. and g–i), j–l) the corresponding fluorescence images of the nucleus with DAPI, after incubation of 17 d.

were produced on the hydrogels. On a control hydrogel without RGD, the spheroids did not differentiate. It is known in the literature that hMSCs cultured as spheroids maintain cell-to-cell contact and remain undifferentiated.^[81]

3. Conclusion

Due to the high therapeutic efficiency of hMSCs, they are used in clinical applications. Yet, only hMSCs with intact stemness (immunophenotyping, mechanosensing ability and differentiation potential) are selected for such applications. Therefore, it is crucial to find a substrate that can keep this pluripotency. Another challenge is to regulate hMSCs differentiating into a specific lineage (e.g., adipocytes), which is useful for clinic applications (e.g., soft tissue replacement in reconstructive medicine). In this study, a native cell niche mimicking soft nanocomposite hydrogel with confined RGD spacing and surface morphology was fabricated by click chemistry. The goal of this work was to study the stemness and the differentiation potential of hMSCs on patterned and soft substrates regarding three aspects: surface morphology, ligand spacing, and mechanical properties. After investigating the locomotion of hMSCs on two different patterned surfaces (wrinkled or creased) and assessing the strong attachment of hMSCs on the hydrogels, stemness and differentiation potential were confirmed with an influence of the change in mechanical properties and adhesive peptide organization. The results have demonstrated that the immunophenotyping and mechanosensibility of the hMSCs

remain in the case of a culture on these hydrogels and are lost when cultured on hard surfaces. This suggests that these hydrogels could be an excellent candidate to maintain the cell pluripotency. Overall, this work provides information about the stem cells behavior on soft material mimicking natural cell environments and gives further ideas in development of materials in the field of soft tissue engineering.

4. Experimental Section

Materials: All chemicals were purchased from Sigma (Germany) and used without further purification, unless otherwise noted. α -Amino- ω -azido PEG, PEG-MW. 3000, 10 000 Dalton was from RAPP Polymer (Germany). H-Arg-Gly-Asp-Cys-OH trifluoroacetate salt was from Bachem. Dendritic polyglycerol with a number average molecular weight (M_n) of 10 kDa and gold nanoparticles with an average size of 20 nm were synthesized as previously reported.^[46,47]

Cell Culture: hMSCs were purchased from EMD Millipore (Darmstadt, Germany) and cultured in DMEM (Gibco) supplemented with 10% bovine growth serum (Gibco) and 1% penicillin/streptomycin (Gibco) at 37 °C with 5% CO₂. The osteogenic differentiation medium (ODM) and adipogenic differentiation medium (ADM) were obtained from Thermo Fisher (A1007201, A1007001). The fifth to sixth passages of hMSCs were used in this study.

Cell Viability: The viability of hMSCs on the hydrogels was measured by live/dead assay using a LIVE/DEAD kit (Thermo Fisher) after 48 h. Briefly, the live/dead dye solution was prepared by mixing 20 μ L of 2×10^{-3} M EthD-1 stock solution and 5 μ L of 4×10^{-3} M calcein AM into 10 mL of Dulbecco's phosphate-buffered saline (DPBS). Cells were stained by replacing culture medium with 150 μ L of the live/dead dye solution and incubated at 37 °C in the dark for 30 min. Afterwards, the

cells were imaged using an inverted fluorescence microscope. The cell viability was quantified by Cell Counting Kit-8 (CCK-8). 10 μL of CCK-8 solution was added to each well containing cells, and the well plate was continuously incubated at 37 $^{\circ}\text{C}$ for 2 h. Then the OD value for each well was read at wavelength 450 nm to determine the cell viability on a microplate reader. The assay was repeated three times. The cell viability was calculated as following: cell viability (%) = (OD (experiment) – OD (blank))/(OD (control) – OD (blank) \times 100).

Cell Spreading Study: hMSCs were seeded in a 24-well culture plate containing a 12 mm diameter coverslip coated with a hydrogel film in growth medium for 4 h. Then the samples were washed once with the cell culture medium and twice with PBS (pH 7.4), followed by fixing with 4% paraformaldehyde (Sigma, Germany) at room temperature for 30 min. Then, the samples were washed three times with PBS (pH 7.4). For permeabilization purposes, cells were treated with 0.25% (v/v) Triton-X 100 (Sigma, Germany) in PBS for 10 min at room temperature, followed by washing with PBS to remove the detergent. The samples were then incubated with 1% (w/v) bovine serum albumin (BSA) in PBST (0.1% v/v Triton-X 100 in PBS) at room temperature for 45 min to block nonspecific antibody binding. After a brief washing twice with PBST and three times with PBS (pH 7.4), the cells were incubated in the dark for 1 h in a solution of rhodamine phalloidin (1:500 dilution, Life Technologies, ThermoFisher Scientific, USA) and DAPI (1:1000 dilution, Life Technologies, ThermoFischer Scientific, USA). Finally, the samples were washed twice with PBS and were imaged under an inverted fluorescence microscope.

Immunostaining: hMSCs were seeded in a 24-well culture plate containing a 12 mm diameter coverslip coated with a hydrogel film in growth medium for 7 d and then the samples were washed once with the cell culture medium and twice with PBS (pH 7.4). hMSCs were fixed by treatment with 4% paraformaldehyde (PFA) for 30 min. For permeabilization purposes, cells were treated with 0.25% (v/v) Triton-X 100 (Sigma, Germany) in PBS for 1 h at room temperature, followed by washing with PBS (pH 7.4) to remove the detergent. The samples were then incubated with 1% (w/v) bovine serum albumin (BSA) in PBST (0.1% v/v Triton-X 100 in PBS) at room temperature for 1 h to block nonspecific antibody binding. After a brief washing with PBST, the samples were incubated with CD73 monoclonal antibody (AD2), APC, eBioscience diluted at a 1:20 (v/v) ratio or CD90 (Thy-1) monoclonal antibody (eBio5E10 (5E10)), PE, eBioscience diluted at a 1:20 (v/v) ratio, and CD105 monoclonal antibody, FITC (Abcam) diluted at a 1:150 (v/v) ratio in PBST with 1% BSA for overnight at 4 $^{\circ}\text{C}$ in the dark. Afterwards, the samples were washed twice with PBST and three times with PBS (pH 7.4). Finally, the samples were imaged under a confocal microscope.

YAP Nuclear Localization: hMSCs were seeded in a 24-well culture plate containing a 12-mm diameter coverslip coated with a hydrogel film in growth medium for 7 d and then the samples were washed once with the cell culture medium and twice with PBS (pH 7.4). hMSCs were fixed by treatment with 4% paraformaldehyde (PFA) for 30 min. For permeabilization purposes, cells were treated with 0.25% (v/v) Triton-X 100 (Sigma, Germany) in PBS for 10 min at room temperature, followed by washing with PBS to remove the detergent. The samples were then incubated with 1% (w/v) bovine serum albumin (BSA) in PBST (0.1% v/v Triton-X 100 in PBS) at room temperature for 45 min to block nonspecific antibody binding. After a brief washing with PBST, the samples were incubated with a primary antibody monoclonal anti-YAP (YAP antibody #4912, Cell Signaling Technology) diluted at a 1:200 (v/v) ratio in PBST with 1% BSA for 1 h at room temperature. Afterwards, the samples were washed twice with PBST and three times with PBS and were then incubated in the dark overnight with a fluorescently labeled secondary antibody (goat anti-rabbit IgG secondary antibody, Alexa Fluor 568), then washed three times with PBS and incubated for another 1 h in a solution of FITC-conjugated phalloidin (1:500 dilution, Life Technologies, ThermoFisher Scientific, USA) and DAPI (1:500 dilution). Finally, the samples were washed twice with PBS and were imaged under a confocal microscope. DAPI and FITC phalloidin channels were used to identify the nuclear and cytoplasmic region of each cell in a single imaging plane. Using the YAP fluorescent channel, the average YAP

intensity in the nuclear and cytoplasmic areas was calculated for each cell with at least 40 cells. Next, the YAP nuclear to cytoplasmic ratio was calculated as the average YAP intensity in the nucleus divided by the average YAP intensity in the cytoplasm.

Differentiation Assay: hMSCs were seeded in a 24-well plate containing a 12-mm diameter coverslip coated with a thin hydrogel film in growth medium for 7 d and then incubated with differentiation media for adipogenic or osteogenic differentiation. hMSCs cultured only in growth media were negative controls. After incubation of the cells for adipogenic and osteogenic differentiation for 17 d, osteoblasts were assessed with APL and adipocytes were assessed with oil red O solution. Images were then captured with an inverted fluorescence microscope.

SEM Imaging: hMSCs were seeded in a 12-well culture plate containing a 1 \times 1 cm^2 silanized glass slide coated with a thin hydrogel film and in growth medium for 24 h and then fixed with 4% paraformaldehyde (Sigma, Germany) at room temperature for 15 min. Then, the samples were washed three times with PBS (pH 7.4). hMSC cultured in bare glass were used as controls. Prior to SEM measurements, gradual dehydration was performed to get rid of the water by immersing each sample in ethanol solutions from a low concentration (50%, 60%, 75%, 90%) to the highest concentration (100%) for 15 min at each concentration. The samples underwent gold sputtering before SEM measurements. The samples were gold coated by using an Edwards S150A sputter coater with gold deposition rate of 15 nm min^{-1} for 30 s. The SEM images were then recorded with a scanning electron microscopy (SEM, SU8030, Hitachi, Germany).

Statistical Analysis: *p*-values were calculated using Student *t*-test and the following increments of increasing significance: *p* > 0.05 (ns, not significant); *p* \leq 0.05 (*); *p* \leq 0.01 (**); *p* \leq 0.001 (***); *p* \leq 0.0001 (****). Error bars in figures represent the standard deviation from the mean.

Atomic Force Microscopy: Morphologies of different hydrogels thin films were studied by AFM imaging in dry and liquid conditions in PeakForce mode. Maximum applied forces of 500–1000 pN were used when measured in Milli-Q. All AFM imaging of hydrogels were conducted with a Multimode 8 from Bruker with a J scanner and a Nanoscope V controller. Samples were measured inside a fluid chamber at room temperature. For determination of changes in film thickness and degree of hydrogel swelling from dry to liquid state, the scratch method was used. 70 \times 70 μm regions with the scratch in the middle (see Figure S8, Supporting Information) were scanned in contact mode using a minimal optimized loading force set point value in combination with slow scan rates of about 0.3 Hz in order to reduce shear forces. To observe changes in hydrogel surface morphology from micro to nanoscale, images were taken with scan sizes of 10, 5, and 1 μm and a resolution of 512 points per line and 0.7 Hz scan rate. Imaging was performed with SNL-10 tips A from Bruker, model SNL-10 with nominal tip radius of 2 nm. Surface parameters were obtained using the NanoScope Analysis software version 1.4. Root mean square roughness (R_q) and maximal roughness (R_{max}) were obtained using the cross-section tool from five different regions.

Mechanical Testing with Atomic Force Microscopy: Colloidal force spectroscopy was applied with a 23 μm silica colloid glued with epoxy (UHU 2-komponent Endfest, Germany) to the end of a tipless cantilever F model MLCT-O10 from Bruker with nominal spring constant $k = 0.6 \text{ N m}^{-1}$. Cantilevers were calibrated after functionalization with the colloid in Milli-Q, by compressing on a hard surface of cleaved mica to extract the cantilever's sensitivity, followed by the thermal noise method to obtain the spring constant of the cantilever+colloid system. Force–distance curves were then taken as a control reference on hard mica before each hydrogel surface was tested. Hydrogels were compressed at different locations through approach–retraction cycles with a velocity of 500 nm s^{-1} and maximal loading forces of 10 nN. All CFS experiments were performed in a Nanowizard 4 from JPK in force spectroscopy mode. All obtained force–distance curves were base line and tip-deflection corrected, so that curves were transformed into force–separation curves and used for further calculations. The Young's modulus of hydrogels was calculated with the JPKSPM data processing software using the model of

contact of Hertz for the first 20 nm of deformation following the contact point between colloid and hydrogel surface. For the case of bare AFM tip nanoindentations, the AFM tip is considered as a cone with a 20° opening half-angle and the Sneddon model was applied within the first 50 nm of hydrogel deformation.

Rheology: Rheological data were measured with a Malvern Instruments Kinexus equipped with a parallel plate geometry and with an 8 mm plate-plate. The temperature was kept at 25 °C for all experiments and an average normal force of ≈0.07 N. A solvent trap was used to prevent evaporation. All rheological experiments were repeated three times. $E = 2G'(1 + \nu)$ with Poisson's ratio $\nu = 0.5$ for such hydrogels, with E being the Young's modulus and G' being the elastic modulus.

Supporting Information

Supporting Information is available from the Wiley Online Library or from the author.

Acknowledgements

The authors thank Cathleen Schlesener (Freie Universität of Berlin) for the synthesis of dendritic polyglycerol. The authors acknowledge the assistance of the Core Facility BioSupraMol supported by the DFG. The authors thank the Helmholtz Graduate School of Macromolecular Bioscience and the Dahlem Research School of the Freie Universität Berlin for the financial support. The authors acknowledge Dr. Pamela Winchester for language polishing the manuscript.

Conflict of Interest

The authors declare no conflict of interest.

Keywords

dendritic polyglycerol, gold nanoparticles, human mesenchymal stem cells, nanocomposites, polyethylene glycol

Received: June 28, 2019

Revised: October 1, 2019

Published online: October 31, 2019

- [1] B. M. Abdallah, M. Kassem, *Gene Ther.* **2007**, *15*, 109.
- [2] H. J. Kim, J.-S. Park, *Dev. Reprod.* **2017**, *21*, 1.
- [3] L. Bagno, K. E. Hatzistergos, W. Balkan, J. M. Hare, *Mol. Ther.* **2018**, *26*, 1610.
- [4] A. J. Rosenbaum, D. A. Grande, J. S. Dines, *Organogenesis* **2008**, *4*, 23.
- [5] A. I. Caplan, *J. Cell. Physiol.* **2007**, *213*, 341.
- [6] Y. Jung, H. Ji, Z. Chen, H. Fai Chan, L. Atchison, B. Klitzman, G. Truskey, K. W. Leong, *Sci. Rep.* **2015**, *5*, 15116.
- [7] H. Iijima, T. Isho, H. Kuroki, M. Takahashi, T. Aoyama, *npj Regener. Med.* **2018**, *3*, 15.
- [8] M. Wu, R. Zhang, Q. Zou, Y. Chen, M. Zhou, X. Li, R. Ran, Q. Chen, *Sci. Rep.* **2018**, *8*, 5014.
- [9] K. S. Lalykina, N. V. Latsinik, S. I. Epikhina, Fridenshtein, *Bull. Exp. Biol. Med.* **1976**, *81*, 239.
- [10] H. J. Anderson, J. K. Sahoo, R. V. Ulijn, M. J. Dalby, *Front. Bioeng. Biotechnol.* **2016**, *4*, 38.
- [11] W. L. Murphy, T. C. McDevitt, A. J. Engler, *Nat. Mater.* **2014**, *13*, 547.
- [12] A. J. Engler, S. Sen, H. L. Sweeney, D. E. Discher, *Cell* **2006**, *126*, 677.
- [13] J. H. Wen, L. G. Vincent, A. Fuhrmann, Y. S. Choi, K. C. Hribar, H. Taylor-Weiner, S. Chen, A. J. Engler, *Nat. Mater.* **2014**, *13*, 979.
- [14] Z. Liu, W. Toh, T. Y. Ng, *Int. J. Appl. Mech.* **2015**, *07*, 1530001.
- [15] Y. Peng, Q.-J. Liu, T. He, K. Ye, X. Yao, J. Ding, *Biomaterials* **2018**, *178*, 467.
- [16] K. Ye, L. Cao, S. Li, L. Yu, J. Ding, *ACS Appl. Mater. Interfaces* **2016**, *8*, 21903.
- [17] E. Sharon, M. Marder, H. Swinney, *Am. Sci.* **2004**, *92*, 254.
- [18] R. Peng, X. Yao, J. Ding, *Biomaterials* **2011**, *32*, 8048.
- [19] X. Yao, R. Peng, J. Ding, *Adv. Mater.* **2013**, *25*, 5257.
- [20] T. Tallinen, J. Y. Chung, J. S. Biggins, L. Mahadevan, *Proc. Natl. Acad. Sci. USA* **2014**, *111*, 12667.
- [21] J. A. Howarter, C. M. Stafford, *Soft Matter* **2010**, *6*, 5661.
- [22] B. Li, Y.-P. Cao, X.-Q. Feng, H. Gao, *Soft Matter* **2012**, *8*, 5728.
- [23] R. Takahashi, Y. Ikura, D. R. King, T. Nonoyama, T. Nakajima, T. Kurokawa, H. Kuroda, Y. Tonegawa, J. P. Gong, *Soft Matter* **2016**, *12*, 5081.
- [24] M. Kato, Y. Tsuboi, A. Kikuchi, T.-A. Asoh, *J. Phys. Chem. B* **2016**, *120*, 5042.
- [25] C. Yang, N. Hu, W. Wang, B. Cao, *J. Power Sources* **2018**, *399*, 115.
- [26] D. Xia, L. M. Johnson, G. P. Lopez, *Adv. Mater.* **2012**, *24*, 1287.
- [27] M. Guvendiren, S. Yang, J. A. Burdick, *Adv. Funct. Mater.* **2009**, *19*, 3038.
- [28] T. Razafiarison, C. N. Holenstein, T. Stauber, M. Jovic, E. Vertudes, M. Loparic, M. Kawecki, L. Bernard, U. Silvan, J. G. Snedeker, *Proc. Natl. Acad. Sci. USA* **2018**, *115*, 4631.
- [29] M. Guvendiren, J. A. Burdick, *Biomaterials* **2010**, *31*, 6511.
- [30] S. K. Kureel, P. Mogha, A. Khadpekar, V. Kumar, R. Joshi, S. Das, J. Bellare, A. Majumder, *Biol. Open* **2018**, *8*, 364059.
- [31] V. V. Rao, M. K. Vu, H. Ma, A. R. Killars, K. S. Anseth, *Bioeng. Transl. Med.* **2019**, *4*, 51.
- [32] I. Levental, P. C. Georges, P. A. Janmey, *Soft Matter* **2007**, *3*, 299.
- [33] R. Randriantsilefisoa, J. L. Cuellar-Camacho, M. S. Chowdhury, P. Dey, U. Schedler, R. Haag, *J. Mater. Chem. B* **2019**, *7*, 3220.
- [34] M. C. Lensen, V. A. Schulte, M. Diez, in *Biomaterials – Physics and Chemistry* (Ed: R. Pignatello), InTech, UK **2011**, pp. 1–18.
- [35] X. Wang, S. Li, C. Yan, P. Liu, J. Ding, *Nano Lett.* **2015**, *15*, 1457.
- [36] J. Huang, S. V. Grater, F. Corbellini, S. Rinck, E. Bock, R. Kemkemer, H. Kessler, J. Ding, J. P. Spatz, *Nano Lett.* **2009**, *9*, 1111.
- [37] K. Ye, X. Wang, L. Cao, S. Li, Z. Li, L. Yu, J. Ding, *Nano Lett.* **2015**, *15*, 4720.
- [38] L. Dykman, N. Khlebtsov, *Chem. Soc. Rev.* **2012**, *41*, 2256.
- [39] S. Li, X. Wang, B. Cao, K. Ye, Z. Li, J. Ding, *Nano Lett.* **2015**, *15*, 7755.
- [40] B. L. Ekerdt, R. A. Segalman, D. V. Schaffer, *Biotechnol. J.* **2013**, *8*, 1411.
- [41] P. Thoniyot, M. J. Tan, A. A. Karim, D. J. Young, X. J. Loh, *Adv. Sci.* **2015**, *2*, 1400010.
- [42] J. H. Choi, J. M. Gimble, K. Lee, K. G. Marra, J. P. Rubin, J. J. Yoo, G. Vunjak-Novakovic, D. L. Kaplan, *Tissue Eng., Part B* **2010**, *16*, 413.
- [43] A. Casadei, R. Epis, L. Ferroni, I. Tocco, C. Gardin, E. Bressan, S. Sivolella, V. Vindigni, P. Pinton, G. Mucci, B. Zavan, *J. Biomed. Biotechnol.* **2012**, *2012*, 12.
- [44] K. Hemmrich, D. von Heimbürg, *Expert Rev. Med. Devices* **2006**, *3*, 635.
- [45] I. Van Nieuwenhove, L. Tytgat, M. Ryx, P. Blondeel, F. Stillaert, H. Thienpont, H. Ottevaere, P. Dubruel, S. Van Vlierberghe, *Acta Biomater.* **2017**, *63*, 37.
- [46] R. A. Gittens, T. McLachlan, R. Olivares-Navarrete, Y. Cai, S. Berner, R. Tannenbaum, Z. Schwartz, K. H. Sandhage, B. D. Boyan, *Biomaterials* **2011**, *32*, 3395.
- [47] X. Hu, S.-H. Park, E. S. Gil, X.-X. Xia, A. Weiss, D. Kaplan, *Biomaterials* **2011**, *32*, 8979.
- [48] R. Randriantsilefisoa, J. L. Cuellar-Camacho, M. S. Chowdhury, P. Dey, U. Schedler, R. Haag, *J. Mater. Chem. B* **2019**, *7*, 3220.

- [49] K. Saha, J. Kim, E. Irwin, J. Yoon, F. Momin, V. Trujillo, D. V. Schaffer, K. E. Healy, R. C. Hayward, *Biophys. J.* **2010**, *99*, L94.
- [50] R. Sunyer, A. J. Jin, R. Nossal, D. L. Sackett, *PLoS One* **2012**, *7*, e46107.
- [51] V. Trujillo, J. Kim, R. C. Hayward, *Soft Matter* **2008**, *4*, 564.
- [52] E. Martinez-Campos, A. Gallardo, N. Lujan, A. Santos-Coquillat, H. Reinecke, A. del Campo, J. Rodriguez-Hernandez, *ACS Appl. Bio Mater.* **2019**, *2*, 654.
- [53] C.-M. Chen, S. Yang, *Polym. Int.* **2012**, *61*, 1041.
- [54] E. P. Chan, A. J. Crosby, *Soft Matter* **2006**, *2*, 324.
- [55] S. Yokoyama, T. S. Matsui, S. Deguchi, *Biochem. Biophys. Res. Commun.* **2017**, *482*, 975.
- [56] N. D. Evans, E. Gentleman, *J. Mater. Chem. B* **2014**, *2*, 2345.
- [57] X. Trepate, Z. Chen, K. Jacobson, *Compr. Physiol.* **2012**, *2*, 2369.
- [58] X. Wang, X. Hu, I. Dulińska-Molak, N. Kawazoe, Y. Yang, G. Chen, *Sci. Rep.* **2016**, *6*, 28708.
- [59] R. J. Pelham, Y.-L. Wang, *Proc. Natl. Acad. Sci. USA* **1997**, *94*, 13661.
- [60] U. S. Schwarz, J. R. D. Soiné, *Biochim. Biophys. Acta, Mol. Cell Res.* **2015**, *1853*, 3095.
- [61] S. V. Plotnikov, A. M. Pasapera, B. Sabass, C. M. Waterman, *Cell* **2012**, *151*, 1513.
- [62] B. L. Bangasser, S. S. Rosenfeld, D. J. Odde, *Biophys. J.* **2013**, *105*, 581.
- [63] S. Lavenus, P. Pilet, J. Guicheux, P. Weiss, G. Louarn, P. Layrolle, *Acta Biomater.* **2011**, *7*, 1525.
- [64] J. Huang, J. Ding, *Soft Matter* **2010**, *6*, 3395.
- [65] J. E. Frith, R. J. Mills, J. J. Cooper-White, *J. Cell. Sci.* **2012**, *125*, 317.
- [66] Z. Ma, D. N. LeBard, S. M. Loverde, K. A. Sharp, M. L. Klein, D. E. Discher, T. H. Finkel, *PLoS One* **2014**, *9*, e112292.
- [67] M. Dominici, K. Le Blanc, I. Mueller, I. Slaper-Cortenbach, F. Marini, D. Krause, R. Deans, A. Keating, D. Prockop, E. Horwitz, *Cytotherapy* **2006**, *8*, 315.
- [68] K. M. Panchalingam, S. Jung, L. Rosenberg, L. A. Behie, *Stem Cell Res. Ther.* **2015**, *6*, 225.
- [69] A. A. Nery, I. C. Nascimento, T. Glaser, V. Bassaneze, J. E. Krieger, H. Ulrich, *Cytometry, Part A: J. Int. Soc. Anal. Cytol.* **2013**, *83*, 48.
- [70] I. Ullah, R. B. Subbarao, G. J. Rho, *Biosci. Rep.* **2015**, *35*, e00191.
- [71] J. Galipeau, L. Sensebe, *Cell Stem Cell* **2018**, *22*, 824.
- [72] A. Moreira, S. Kahlenberg, P. Hornsby, *J. Mol. Endocrinol.* **2017**, *59*, R109.
- [73] T. Bonfield, M. Majumder, J. Jensen, M. Gilkey, D. Velasquez, S. Oo, M. Sutton, S. Kaur, D. Fletcher, R. vanHeeckeren, R. Somoza, L. Auster, A. Caplan, *Am. J. Respir. Crit. Care Med.* **2017**, *195*, A4319.
- [74] D. K. Yi, S. S. Nanda, K. Kim, S. Tamil Selvan, *J. Mater. Chem. B* **2017**, *5*, 9429.
- [75] R. Yagi, L. F. Chen, K. Shigesada, Y. Murakami, Y. Ito, *EMBO J.* **1999**, *18*, 2551.
- [76] K. H. Wrighton, *Nat. Rev. Mol. Cell Biol.* **2011**, *12*, 404.
- [77] A. M. Loye, E. R. Kinser, S. Bensouda, M. Shayan, R. Davis, R. Wang, Z. Chen, U. D. Schwarz, J. Schroers, T. R. Kyriakides, *Sci. Rep.* **2018**, *8*, 8758.
- [78] H. Song, W. Chang, B.-W. Song, K.-C. Hwang, *Am. J. Stem Cells* **2011**, *1*, 22.
- [79] R. Peng, X. Yao, B. Cao, J. Tang, J. Ding, *Biomaterials* **2012**, *33*, 6008.
- [80] X. Wang, C. Yan, K. Ye, Y. He, Z. Li, J. Ding, *Biomaterials* **2013**, *34*, 2865.
- [81] G. R. Souza, J. R. Molina, R. M. Raphael, M. G. Ozawa, D. J. Stark, C. S. Levin, L. F. Bronk, J. S. Ananta, J. Mandelin, M. M. Georgescu, J. A. Bankson, J. G. Gelovani, T. C. Killian, W. Arap, R. Pasqualini, *Nat. Nanotechnol.* **2010**, *5*, 291.